https://doi.org/10.5194/tc-2022-118
Preprint. Discussion started: 20 July 2022

The Cryosphere Discussions

Characteristics of the contemporary Antarctic firn layer simulated with IMAU-FDM v1.2A (1979-2020)

Sanne B.M. Veldhuijsen[1], Willem Jan van de Berg[1], Max Brils[1], Peter Kuipers Munneke[1], and Michiel R. van den Broeke[1]

[1]Institute for Marine and Atmospheric Research Utrecht, Utrecht University, Utrecht, The Netherlands

Correspondence: Sanne B.M. Veldhuijsen (s.b.m.veldhuijsen@uu.nl)

Abstract. Firn simulations are essential for understanding Antarctic ice sheet mass change as they enable us to convert satellite altimetry observed volume changes to mass changes, and to quantify the meltwater buffering capacity of firn. Here, we present and evaluate a simulation of the contemporary Antarctic firn layer using the updated semi-empirical firn model IMAU-FDM for the period 1979-2020. In IMAU-FDM, we have improved the fresh snow density and firn compaction parameterizations, and used improved atmospheric forcing. In addition, the model has been tuned and evaluated against 148 in situ observations across the ice sheet. The updated model captures the observed strong spatial variation in firn thickness and density. The temporal variation can be split into a rather stable seasonal cycle driven by snowfall, compaction and melt seasonal cycles, and more irregular decadal variations driven by snowfall anomalies. Comparison of simulated surface elevation change with altimetry shows that the decadal trends agree reasonably well, and that the performance of the updated model has improved, notably in Dronning Maud Land and Wilkins Land.

1 Introduction

The Antarctic ice sheet (AIS) is the largest freshwater reservoir on Earth, and is losing mass since at least 2002 (Shepherd et al., 2018; Rignot et al., 2019), thereby contributing to around 10 % of global average sea level rise since 1993 (Oppenheimer et al., 2019). About 99 % of the AIS is covered by a firn layer (Winther et al., 2001), which represents the transition of fresh snow to glacier ice. The firn layer thickness typically ranges from 40 m in the coastal zone to 100 m in the interior (van den Broeke, 2008), and also fluctuates in time due to changes in accumulation, melt and firn compaction. A detailed understanding of the firn layer and its variability is important for constraining current and future AIS mass change for two key reasons. Firstly, firn depth and density estimates are required to convert altimetry observed volume-to-mass changes, which remains a major source of uncertainty in mass balance studies (Verjans et al., 2021). Secondly, firn provides pore space in which nearly all (>98 %) the surface meltwater refreezes or is retained, thereby buffering surface meltwater and preventing mass loss by runoff of surface meltwater (Medley et al., 2020).

From both observational and modelling studies, firn layer depth and density are known to vary greatly across the AIS, resulting from the wide range of (near) surface climatic conditions (e.g., Keenan et al., 2021), i.e. temperature, wind speed, accumulation and melt. Low temperatures in the interior (Fig. 1) cause slow densification rates resulting in a firn layer thickness

https://doi.org/10.5194/tc-2022-118
Preprint. Discussion started: 20 July 2022


The Cryosphere Discussions

(defined here as the depth of the 830 $\mathrm{kg\,m^{-3}}$ density level) greater than 100 m. On the other hand, on warm and dry ice shelves, densification and melt is enhanced, resulting in denser firn layers with a depth less than 50 m (van den Broeke, 2008).

Changes in the AIS surface elevation are used as measures of its dynamics and mass balance. The difficulty is that these seasonal cycles and decadal changes in elevation are not solely caused by fluctuations in mass, but also for a large part by fluctuations in the firn density (Ligtenberg et al., 2012; Medley et al., 2020). In altimetry studies, it is therefore important to accurately separate these changes in a mass and density component. The mass component can subsequently be separated in an ice-dynamical and a surface mass balance component (Willen et al., 2021).

Another important characteristics of the firn layer is its capability to retain meltwater in pore spaces by capillary forces and refreezing. In a warmer future climate, reduced accumulation, enhanced firn compaction, melt, and refreezing can all lead to firn air depletion, thereby limiting the meltwater storage capacity of the firn and promoting hydrofracturing-induced ice shelf collapse (Munneke et al., 2014; Datta et al., 2019), contributing to future Antarctic mass loss and sea level rise (Gilbert and Kittel, 2021). Accurate information about firn conditions is thus essential both for understanding both the current AIS mass balance, and to predict its future.

Firn models can fill spatial and temporal gaps between the relatively sparse observations from firn cores and snow pits. While remote sensing products provide high temporal and spatial resolution information about surface height changes, and indirectly, firn properties of the top few meters (e.g., Davis and Poznyak, 1993; Schröder et al., 2019; Shepherd et al., 2019), they do not provide information about the deeper firn column. Firn models are, therefore, also important to obtain vertical variations in density, and can be used to perform future simulations of firn depth and density in response to climate change scenarios (Ligtenberg et al., 2012; Munneke et al., 2014).

Firn models can roughly be divided in two classes: physically based and semi-empirical models. Semi-empirical models neglect some processes such as drifting-snow compaction (e.g., Sommer et al., 2018) and use a larger degree of tuning to observations representative of the past or present climate, which might be not representative under future climatic conditions. Nevertheless, semi-empirical models require less poorly known parameters, such as roughness length, snow grain shape and size, and computational demands are lower (Keenan et al., 2021). This is especially advantageous for data-scarce regions and large-scale studies. Therefore, semi-empirical firn models have been used widely for correction of satellite altimetry products (e.g., Schröder et al., 2019; Smith et al., 2020; Willen et al., 2021) and to assess the meltwater buffering capacity of the Antarctic firn layer (Ligtenberg et al., 2014; Munneke et al., 2014). Several studies have found that the performance of semi-empirical models is comparable to that of physically based models (Steger et al., 2017; Vandecrux et al., 2020; Keenan et al., 2021).

Differences in the formulations of, e.g., firn densification and fresh snow density can lead to a substantial spread between modelled firn thickness and air content. Using statistical emulation of firn densification models, Verjans et al. (2021) quantified how much different sources of uncertainty contribute to the total uncertainty in modelled firn thickness change of the East Antarctic ice sheet. At the basin scale, the ensemble uncertainty in firn thickness changes ranges from 0.2 to 1.0 $\mathrm{cm\,yr^{-1}}$, which amounts to a 15-300 % relative uncertainty. While differences in climate forcing have the largest influence on the spread, in basins with high snowfall and a large spatial variability of climatic conditions firn densification formulation also has

https://doi.org/10.5194/tc-2022-118
Preprint. Discussion started: 20 July 2022


The Cryosphere Discussions

Table 1. Abbreviations of IMAU-FDM versions used in this study.

Abbreviation	IMAU-FDM version	Forcing	Other
FDM v1.2A	FDM v1.2 Antarctica	RACMO2.3p2, ERA-5	-
FDM FS-K	FDM v1.2 Antarctica	RACMO2.3p2, ERA-5	Fresh snow density of Kaspers et al. (2004)
FDM FS-L	FDM v1.2 Antarctica	RACMO2.3p2, ERA-5	Fresh snow density of Lenaerts et al. (2012)
FDM v1.2A-log	FDM v1.2 Antarctica	RACMO2.3p2, ERA-5	Power MO_{830} fit
FDM v1.1p1	FDM v1.1	RACMO2.3p1, ERA-Interim	-
FDM v1.1p2	FDM v1.1	RACMO2.3p2, ERA-5	-

a substantial contribution to the spread (up to 46 %). In basins with recent increases in snowfall rates the contribution of fresh snow density to the total uncertainty is also substantial (up to 28 %).

In this study, we have improved the semi-empirical IMAU Firn Densification model (IMAU-FDM) (Ligtenberg et al., 2011) by updating the (i) fresh snow density, (ii) firn densification parameterizations, and (iii) by using updated atmospheric forcing fields. In addition, the model has been retuned against 148 field measurements across the AIS. This version 1.2A of IMAU-FDM supersedes the previous version (Ligtenberg et al., 2011). Here, we present the simulated contemporary characteristic of the Antarctic firn layer for the period 1979-2020. We focus on spatial, seasonal and decadal variability in firn thickness and firn air content. To evaluate the decadal surface elevation changes and seasonal cycles we compare the simulations to remote sensing altimetry. Finally, we test how sensitive the modelled firn layer is to uncertainties in model variables.

2 Materials and methods

2.1 IMAU-FDM

IMAU-FDM is a semi-empirical 1D firn densification model that simulates the time evolution of firn density, temperature, liquid water content and surface height changes due to firn and SMB processes. The model employs up to 3000 layers of 3 to 15 cm thickness, which represent the firn properties in a Lagrangian way. The model was originally developed by Helsen et al. (2008), and updated by Ligtenberg et al. (2011) to a version abbreviated here to FDM v1.1. Brils et al. (2021) recently improved IMAU-FDM applied to the Greenland ice sheet by including a refined parameterization of the thermal conductivity to version FDM V1.2G. The various versions of IMAU-FDM have been extensively evaluated against firn density and temperature observations from both Greenland and Antarctica (Ligtenberg et al., 2011; Kuipers Munneke et al., 2015; Brils et al., 2021). The performance of these IMAU-FDM versions in Greenland as well as in Antarctica was found to be comparable to that of the more physically based SNOWPACK model (Steger et al., 2017; Vandecrux et al., 2020; Keenan et al., 2021). We further improved IMAU-FDM for Antarctica to FDM v1.2A by updating the (i) fresh snow density parameterization and (ii) firn densification, as discussed below. Abbrevations of all versions of IMAU-FDM used in this study are listed in Table 1.

https://doi.org/10.5194/tc-2022-118
Preprint. Discussion started: 20 July 2022


The Cryosphere Discussions
Open Access
EGU

2.1.1 Fresh snow density

The fresh snow density (ρ_s; $\mathrm{kg\,m^{-3}}$) is an important, but poorly constrained upper boundary condition of firn models. FDM v1.1 used the fresh snow density parameterization of Kaspers et al. (2004). It varies as a function of annual average surface temperature ($\bar{T}_s$; K), 10-m wind speed ($\bar{V}_{10}$; $\mathrm{m\,s^{-1}}$) and accumulation ($\dot{b}$; $\mathrm{mm\,w.e.\,yr^{-1}}$):

$$\rho_s = A + B\bar{T}_s + C\bar{V}_{10} + D\dot{b} \tag{1}$$

in which *A*, *B*, *C* and *D* are fit coefficients. Snow crystal size and therefore fresh snow density indeed increase with increasing temperature. Also, strong winds during snowfall cause crystal breaking, thereby reducing the snow effective grain size (Sato et al., 2008), which results in more efficient packing and increased fresh snow densities. However, at least two concerns can be raised against Eq. (1). First, due to the partly similar spatial patterns of accumulation and temperature in Antarctica, a statistical relationship between fresh snow density and accumulation may exist, however this relationship has no physical grounds. Other studies have therefore not found a dependency between annual accumulation and fresh snow density in Antarctica, Greenland and the Alps (Lehning et al., 2002; Fausto et al., 2018; Lenaerts et al., 2012). Second, Eq. (1) neglects the impact of the meteorological conditions at the time of deposition, which can be highly variable in time. Therefore, we tested the more recent parameterization of Lenaerts et al. (2012), in which ρ_s is a function of instantaneous surface temperature (T_s; K) and 10-m wind speed (V_{10}; $\mathrm{m\,s^{-1}}$):

$$\rho_s = A + B\bar{T}_s + C\bar{V}_{10} \tag{2}$$

in which *A*, *B* and *C* are fit coefficients. The resulting density values are representative of the fresh skin layer density, which typically represents the upper few cm of the snowpack. Within days after depositing, the crystal structures of freshly deposited snow break down due to wind and redistribution of drifting snow, which increases the surface snow density (Groot Zwaaftink et al., 2013). IMAU-FDM does not calculate this densification by wind and redistribution of drifting snow. The fit coefficients *A*, *B* and *C* in Eq. (2) are retuned in order to improve the fit with the observed surface snow densities, defined as the top 0.5 m of the firn column to match the observations.

2.1.2 Dry snow densification rate

Over time, the freshly deposited snow becomes denser. The rate of the dry firn densification ($\mathrm{d}\rho/\mathrm{d}t$) is calculated using the semi-empirical equation of Arthern et al. (2010):

$$\frac{\mathrm{d}\rho}{\mathrm{d}t} = D\dot{b}g(\rho_i - \rho)^{\left(\frac{E_c}{RT} - \frac{E_g}{RT_{ave}}\right)} \tag{3}$$

where *D* is a constant, *g* is the gravitational acceleration, ρ_i is the density of ice ($917\ \mathrm{kg\,m^{-3}}$), *R* is the gas constant, ρ is the layer density ($\mathrm{kg\,m^{-3}}$), *T* is the instantaneous layer temperature (K), T_{ave} is the average surface temperature (K), and E_c and E_g are the activation energies for creep ($60\ \mathrm{kJ\,mol^{-1}}$) and grain-growth ($42.4\ \mathrm{kJ\,mol^{-1}}$), respectively. The constant *D* has different values above (0.03) and below (0.07) the critical density level ρ = $550\ \mathrm{kg\,m^{-3}}$ to represent the distinct densification processes.

https://doi.org/10.5194/tc-2022-118
Preprint. Discussion started: 20 July 2022

For $\rho < 550\ \mathrm{kg\,m^{-3}}$, densification mainly occurs by settling and sliding of grains, and for $\rho > 550\ \mathrm{kg\,m^{-3}}$, it mainly occurs by deformation, sublimation and diffusion. By comparing simulated and observed depths (m) of the 550 and 830 $\mathrm{kg\,m^{-3}}$ density levels (z_{550} and z_{830}, respectively) Ligtenberg et al. (2011) found that Eq. (3) requires a correction function, the so-called MO fits (ratio of Modelled to Observed depths), which turn out to depend on the accumulation rate. These MO fits are defined using the ratio between modelled and observed values of z_{550} and z_{830*}, where $z_{830*} = z_{830} - z_{550}$, using a simulation in which Eq. (3) is used without correction fits. Ligtenberg et al. (2011) and Brils et al. (2021) used logarithmic correction functions, thus:

$$\mathrm{MO} = \alpha - \beta \ln(\dot{b}) \tag{4}$$

in which MO is either MO_{550} or MO_{830}, and α and β are fit coefficients which differ for MO_{550} and MO_{830}. In FDM v1.1 a minimum value of 0.25 is imposed on MO_{550} and MO_{830}. For Greenland and Antarctica, different values for α and β have been used to optimize densification. Here, we also tested a power-law function for MO_{830}:

$$\mathrm{MO}_{830} = \delta \dot{b}^{-\epsilon} + \phi \tag{5}$$

in which δ, and ϵ and ϕ are tuning parameters.

2.1.3 Heat conduction, meltwater percolation and refreezing

The conduction of heat is simulated by using a one-dimensional heat transfer equation, which couples vertical heat conduction to temperature gradients through the thermal conductivity of firn. In FDM v1.1 the thermal conductivity is a function of firn density only (Anderson, 1976), and in FDM v1.2 this has been extended to a function of density and temperature (Calonne et al., 2019). Meltwater percolation is simulated using the tipping-bucket method, whereby each firn layer has a maximum irreducible water content that decreases with increasing density (Coléou et al., 1999). The meltwater can percolate through all layers in a single timestep. The meltwater refreezes when it reaches a layer with sufficient available pore space and if the latent heat can be released. To capture the percolation and refreezing of meltwater more accurately, the model timestep is reduced from 3600 to 300 s for locations with the significant melt. Further details and evaluation of heat conduction, percolation and refreezing are provided by Brils et al. (2021).

2.2 Model strategy

An initial firn layer is obtained by spinning up the model over the reference period until the firn layer is in equilibrium with its surface climate. The equilibrium is roughly reached when the entire firn column, defined here as the depth where the density ρ reaches 830 $\mathrm{kg\,m^{-3}}$, is fully refreshed by accumulation. The required spin-up time in years is therefore calculated as the total thickness of the modelled firn layer divided by the annual accumulation (Kuipers Munneke et al., 2015). As no obvious strong long-term trends have been detected in Antarctica's surface climate and SMB during the period 1979-2020 (e.g., Favier et al., 2017; Mottram et al., 2021), and no reliable surface climate fields are available prior 1979, the spin-up forcing is obtained by looping over the 1979-2020 forcing data. Thereby, we make the rather strong assumption that this 42-year period is representative for the past 100-1000 years and that the firn layer is in equilibrium with that climatic period. In the actual

https://doi.org/10.5194/tc-2022-118
Preprint. Discussion started: 20 July 2022

simulation after the spin-up, a minor trend in total firn air content remains, due to increasing air content in the modelled ice below the firn column. This trend is removed prior to further analysis of the results.

2.3 Surface height change

IMAU-FDM quantifies the impact of firn and SMB processes on the depth of the firn layer. The resulting vertical velocity of the firn top surface (dh/dt) is defined as the sum of these components:

$$\frac{\mathrm{d}h}{\mathrm{d}t} = v_{snow} + v_{sub} + v_{snd} + v_{melt} + v_{ice} + v_{fc} + v_{by} \tag{6}$$

where v_{snow} represents the vertical velocity component as a result of snowfall, v_{sub} of sublimation, v_{snd} of snowdrift erosion, v_{melt} of snowmelt, v_{ice} represents the negative contribution to firn depth due to the upward moving firn-ice transition, v_{fc} of firn compaction and v_{by} of buoyancy on floating ice shelves. All components are derived from run-time output of IMAU-FDM. In a steady-state firn layer, the long-term average mass flux through the lower boundary of the firn column equals the mass flux at the upper boundary. v_{ice} is therefore equal to the mean SMB ($\mathrm{kg\,m^{-2}}$) times ρ_{i} of the reference period, but of opposite sign. The minor residual trend in dh/dt due to increasing air content in the ice below the firn layer is added to v_{ice}. v_{by}, only relevant over ice shelves, is equal to the negative change in firn mass divided by the density of sea water.

2.4 RACMO2.3p2 forcing

IMAU-FDM is forced at the upper boundary with 3-hourly fields of snowfall, sublimation, snowdrift erosion, 10-m wind speed, surface temperature, snowmelt and rainfall. In this study, FDM v1.2A is driven with ERA-5 reanalysis data (Hersbach et al., 2020), dynamically downscaled with the regional atmospheric climate model RACMO2.3p2 (Van Wessem et al., 2018). RACMO2.3p2 is run with a horizontal resolution of 27x27 km and the simulation covers the period 1979-2020. RACMO2.3p2 has been thoroughly evaluated for the Antarctic and Greenland ice sheets by Van Wessem et al. (2018); Noël et al. (2018), respectively. In comparison to RACMO2.3p1, RACMO2.3p2 now employs upper-air relaxation, has updated topography, and a retuned cloud scheme and snow properties. The most important effects of these changes are (i) increased snowfall in the interior (ii) reduced snowdrift sublimation and (iii) increased snowmelt (Van Wessem et al., 2018). Several Antarctic studies use output from FDM v1.1 forced with RACMO2.3p2 (e.g., Schröder et al., 2019; Keenan et al., 2021), but the impact of the improved forcing has not yet been described. As snowfall and surface melt are defining drivers of the state of the firn, we also assess the impact of the updated forcing in this paper. In addition to the updates of RACMO2.3p2, previous FDM simulations for Antarctica used dynamically downscaled ERA-Interim reanalysis data, which has been replaced by ERA-5 in 2019. This results in an improved forcing, for example, surface mass balance anomalies in Dronning Maud Land from 2006 to 2018 are better captured in ERA-5 compared to ERA-Interim (Gossart et al., 2019). We expect that forcing differences in e.g. surface mass balance anomalies have a larger impact on the temporal evolution of the surface height compared to adjustments in the fresh snow density and dry snow densification parameterizations (Verjans et al., 2021).

https://doi.org/10.5194/tc-2022-118
Preprint. Discussion started: 20 July 2022

2.5 Observational data

To tune and evaluate the firn model, we collected published firn density profiles from widely varying locations across the AIS (Fig. 1). We used 125 density profiles from firn cores and 8 density profiles from neutron density probe measurements, combining multiple datasets (van den Broeke, 2008; Schwanck et al., 2016; Bréant et al., 2017; Fernandoy et al., 2010; Montgomery et al., 2018; Fourteau et al., 2019; Olmi et al., 2021; Winstrup et al., 2019). The firn cores and neutron density probe measurements are mostly obtained in summer months between 1980 and 2020. For tuning the MO fits, only dry firn cores are used, as Eq. (3) described dry snow densification only. A firn core is considered dry if its location experiences on average less melt than 5 % of the average annual accumulation. For the MO fits, 104 dry firn cores could be used, which improves upon Ligtenberg et al. (2011), who used data from 48 dry firn cores. To evaluate the firn density profiles from the simulation using the derived MO fits, 122 firn cores could be used. For tuning the fresh snow density parameterization, observations of the density of surface snow, defined as the top 0.5 m, from 65 firn cores could be used. Eight additional surface snow density values from density profiles of neutron density probe measurements (Montgomery et al., 2018) were added after the tuning, and are thus only used for evaluation. We used densities of the top 0.5 m, as this depth is representative of many in situ surface snow density measurements, it generally consists of snow from multiple snowfall events, and it captures the densification by wind and redistribution of drifting snow (Brun et al., 1997).

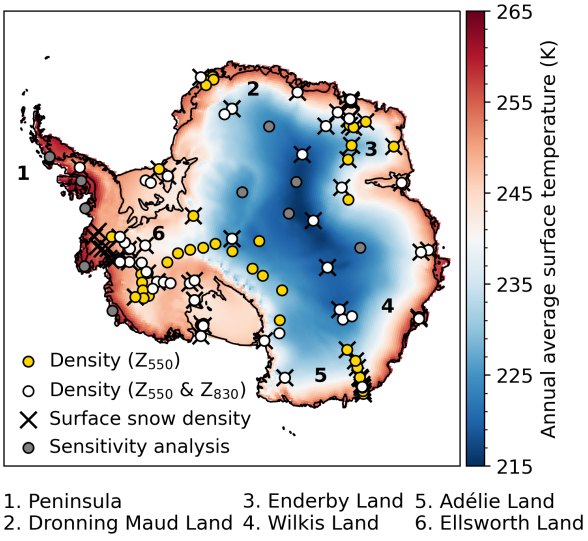

Figure 1. Map of Antarctica showing annual average surface temperature and the locations of the in situ density observations. The yellow circles indicate observational locations of the depths of the critical density level of $\rho = 550\ \mathrm{kg\,m^{-3}}$ (z_{550}), the white circles of the depths of the critical density levels of both $\rho = 550\ \mathrm{kg\,m^{-3}}$ (z_{550}) and $\rho = 830\ \mathrm{kg\,m^{-3}}$ (z_{830}), and the black crosses of the surface snow densities (top 0.5 m of the firn column). The grey circles indicate ten additional locations that were included in the sensitivity analysis (on top of the yellow and white circles). The numbers indicate regions mentioned throughout the manuscript.

https://doi.org/10.5194/tc-2022-118
Preprint. Discussion started: 20 July 2022

In order to verify whether the modelled surface elevation trends and seasonal variability align with observations, we used a multi-mission satellite altimetry product covering the period January 1992 to December 2015 as presented by Schröder et al. (2019). In this product, data from the ERS-1, ERS-2, Envisat, ICESat, and CryoSat-2 missions are combined into a monthly time series on a 10x10 km grid, with the polar gap, floating ice shelves and steep terrain areas being excluded. The altimetry product has been resampled to the FDM grid with the bilinear resampling method. The measurement precision over flat terrain ranges from 5 to 15 cm depending on the satellite. However, as the precision decreases with increasing surface slope, the uncertainty can reach several meters in the coastal regions with steep topography. Offsets due to variations of penetration depth of the radar signals are not included in this estimate. Validation of this dataset with in situ and air borne observations showed that the products are successfully combined (Schröder et al., 2019).

2.6 Sensitivity analysis

To study the model sensitivity to input and parameter uncertainty we performed a sensitivity analysis for the 105 observational locations shown in Figure 1. To improve the representation of high accumulation and low temperature areas, we used 10 additional locations in this analysis (Fig. 1). Verjans et al. (2021) and Lundin et al. (2017) showed that differences in accumulation, temperature, firn densification formulation and fresh snow density can lead to a substantial spread in modelled firn thickness and air content. We performed model sensitivity tests in which these components were separately adjusted by adding and subtracting the estimated uncertainties. The uncertainty in the accumulation forcing was based on the spread of precipitation over the AIS among regional climate models and a re-analysis product (+-8 %) (Mottram et al., 2021). The uncertainty of temperature forcing was based on the evaluation with in situ measurements (+-1.5 K) (Van Wessem et al., 2018). For the uncertainty of the dry snow densification rate, we use the 95 % confidence intervals of the MO fits (Eqs. 4 and 5; Fig. 3). The uncertainty of the fresh snow density was based on evaluation with in situ measurements (30 $\mathrm{kg\,m^{-3}}$; Section 3.2). Another important source of forcing uncertainty is the climate forcing during the spin-up period. As explained in Section 2.2, the spin-up forcing is obtained by looping over the 1979-2020 forcing data. However, firn core (Thomas et al., 2017) and isotopes (Stenni et al., 2017) studies show that in several Antarctic regions, especially the Antartic Peninsula, the accumulation and temperature have been increasing by about 10 % and 1 K over the last centuries. Therefore, we include sensitivity tests in which we adjusted the accumulation and temperature forcing only during the spin-up period. In the accumulation sensitivity test we reduced the accumulation prior to 1895 by 10 %, from 1895 to 1936 by 6.66 % and from 1937 to 1978 by 3.33 %. In the temperature sensitivity test we reduced the temperature prior to 1895 by 1 K, from 1895 to 1936 by 0.66 K and from 1937 to 1978 by 0.33 K. As the uncertainties between temperature and accumulation during the spin-up period are not independent, we also performed a test in which we simultaneously adjusted the temperature and precipitation.

https://doi.org/10.5194/tc-2022-118
Preprint. Discussion started: 20 July 2022

Table 2. Fit coefficients and statistics of the fresh snow density parameterizations (Eqs. 1,2). The fit coefficients of FDM FS-K and FDM FS-L are taken from Kaspers et al. (2004) and Lenaerts et al. (2012), respectively.

Version	A ($kg\,m^{-3}$)	B ($kg\,yr\,m^{-3}\,mm\,w.e.^{-1}$)	C ($kg\,s\,m^{-4}$)	D ($kg\,m^{-3}\,K^{-1}$)	RMSE ($kg\,m^{-3}$)	Bias ($kg\,m^{-3}$)	R^2
FDM FS-K[a]	-77	0.075	1.5	6.8	39.9	18.2	0.39
FDM FS-L[b]	97.5		0.77	4.49	54.5	-44.0	0.40
FDM v1.2A[b]	83		0.77	11.67	29.4	-0.1	0.49

[a]using annual average accumulation, temperature and wind speed. [b]using instantaneous temperature and wind speed.

3 Tuning and model performance

3.1 Fresh snow density

To tune and evaluate the fresh snow density parametrization, we performed simulations with FDM v1.2A using parameterization of Kaspers et al. (2004), Lenaerts et al. (2012) and the latter with updated constants. These simulations are abbreviated as FDM FS-K, FDM FS-L and FDM v1.2A, respectively. The fit coefficients and statistics of the simulations are listed in Table 2. For all sensitivity tests presented here, we calculated the associated MO fits. However, the impact of the different MO fits on the surface snow densities is negligible. Figure 2a shows the modelled against observed surface snow densities for FDM FS-K and FDM v1.2A. FDM FS-K somewhat overestimates the surface snow densities (bias = 18.2 $kg\,m^{-3}$), especially for high surface density. FDM FS-L (not shown) substantially underestimates surface snow densities (bias = -44 $kg\,m^{-3}$), but has a higher correlation with the observations than FDM FS-K. The degree of underestimation increased with increasing wind speed, which suggests that a higher value of fit coefficient C is needed to properly capture the impact of wind compaction. This aligns with the fact that IMAU-FDM does not include densification by wind packing. In the optimized fit coefficients (FDM v1.2A, Table 3) the value of C is 2.6 times higher than the value reported by Lenaerts et al. (2012). The wind dependency is also 2.4 times stronger than proposed by Kaspers et al. (2004), which is in agreement with Sugiyama et al. (2012) who found a factor 2.8. The RMSE of the surface snow density of FDM v1.2A is 26 % lower compared to FDM FS-L, due to both minimizing the bias and improving the representation of the variability. In general, the surface snow density is reduced with 18 $kg\,m^{-3}$, especially in the high accumulation margins, and to a lesser extent in windy escarpment regions (Fig. 2b). The updated parameterization has a similar bias and RMSE to surface snow density observations compared to the SNOWPACK model and the Community Firn Model (CFM) (Keenan et al., 2021; Medley et al., 2020). The fresh snow density parameterization for Greenland used in FDM v1.2G, is only a function of yearly temperature (Brils et al. (2021). This is in contrast with Antarctica, where we found a strong dependency with instantaneous wind speed and temperature, which is in line with previous work (Keenan et al., 2021; Lenaerts et al., 2012; van Kampenhout et al., 2017), and likely owing to the larger range in temperature and wind speed conditions during snow deposition in Antarctica.

https://doi.org/10.5194/tc-2022-118
Preprint. Discussion started: 20 July 2022

The Cryosphere
Discussions
Open Access
EGU

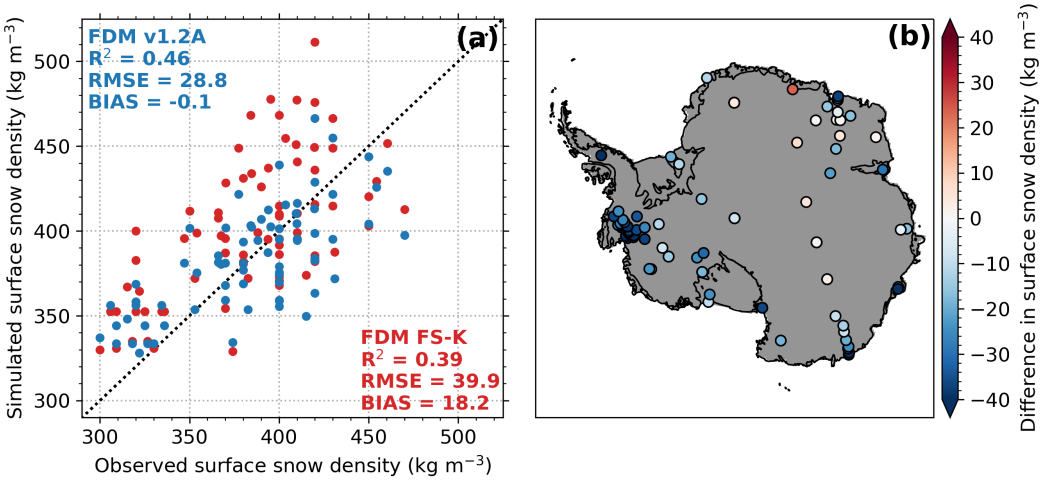

Figure 2. (a) Scatter plot of simulated against observed surface snow density using the fresh snow density expressions of FDM v1.2A and Kaspers et al. (2004) (FDM FS-K). **(b)** Map of average difference between the simulated surface snow densities of the two tests (FDM v1.2A – FDM FS-K) for the locations with observations.

3.2 Dry snow densification rate

To tune and evaluate the dry snow densification rate we first performed a simulation of FDM v1.2A without MO fits. The resulting MO fits and statistics are listed in Table 3 and shown in Figures 3a,b. The optimal MO_{550} fit is less steep than the one found by Ligtenberg et al. (2011). The fresh snow density is now independent of accumulation and generally lower, and hence more densification is needed at high accumulation sites. The update of the fresh snow density leads to a slightly deteriorated correlation for the MO_{550}. For the MO_{830} regression line, we found that a power fit (FDM v1.2A) compared to a logarithmic fit (FDM v1.2A-log) improves correlation (R^2 = 0.88 compared to R^2 = 0.83). Furthermore, a minimum value is now explicitly derived with the power fit, so that a rather arbitrary minimum value no longer needs to be prescribed. When the locations are rerun using the derived MO fits, the resulting RMSE of the modelled z_{830*}, and z_{830} (firn thickness) with the power fit is respectively 25 and 23 % lower compared to the logarithmic fit (Fig. 3c). Using a power fit results in higher MO_{830} values for low (<400 $\mathrm{mm\,yr^{-1}}$) and high (>1,400 $\mathrm{mm\,yr^{-1}}$) accumulation regions, and lower MO_{830} values for intermediate accumulation regions (400-1,400 $\mathrm{mm\,yr^{-1}}$) (Fig. 3b). Therefore, the densification rate is increased in high and low accumulation regions and reduced in intermediate accumulation regions. This results in decreased firn thickness in high and low accumulation regions, and in increased firn thickness in intermediate accumulation regions (Fig. 3d). Especially large differences are found in high accumulation areas where the MO fit curve approaches zero. Differences between the MO fits used for Greenland in FDM v1.2G might partly be related to the fact that dry firn cores in Antarctica cover a larger range of annual average accumulation conditions, 20 to 960 $\mathrm{mm\,yr^{-1}}$ compared to 80 to 680 $\mathrm{mm\,yr^{-1}}$ in Greenland.

https://doi.org/10.5194/tc-2022-118
Preprint. Discussion started: 20 July 2022


The Cryosphere Discussions
Open Access
EGU

Table 3. Fits coefficients and statistics of the MO fits (Eqs. 4,5). The fit coefficients and statistics of FDM v1.1 are taken from Ligtenberg et al. (2011). The FDM v1.2A-log uses the settings of FDM v1.2A; only Eq. (3) is optimized using a logaritmic MO_{830} fit.

Version	Fit	α	β	σ	ϵ	ϕ	RMSE (m)	R^2
MO_{550} FDM v1.1p1	log	1.435	0.151					0.43
MO_{550} FDM v1.2A	log	1288	0.117					0.37
MO_{830} FDM v1.1p1	log	2.366	0.292					0.71
MO_{830} FDM v1.2A-log	log	2.504	0.334				0.13	0.83
MO_{830} FDM v1.2A	power			6.387	0.477	0.195	0.11	0.88

4 Spatial and temporal variability of firn depth and density

4.1 Spatial density variability

Using the improved firn model, we simulate the spatial and temporal patterns of the AIS firn characteristics at 27 km resolution. The spatial patterns of the densities, including values found by field measurements, are shown Figure 4. Figure 4a shows the spatial patterns of the average surface snow density of the top 0.5 m. The patterns are primarily a reflection of the variation in fresh snow density, with the lowest values on the very cold and calm East-Antarctic plateau and higher values in the windy escarpment regions and along the warm coastal margins. On top of this, the surface snow density further increases over the ice shelves and coastal margins, as intermittent melting and refreezing of retained meltwater increases the near-surface density.

The spatial pattern of the depths of the critical density levels z_{550} and z_{830} are shown in Figures 4b and c, and are roughly the inversed pattern of the surface snow density, which constitutes the upper boundary of the depth-density profile. For simplicity, we define the firn thickness as z_{830}. The patterns vary spatially across climatic regions with temperature as a primary driver and accumulation as a secondary driver. The highest z_{550} and z_{830} values are found in the interior, where the densification rate is low due to low temperatures, and the surface snow density is low. Generally, the z_{550} and z_{830} values are low along the warm coast due to faster densification, higher surface snow densities and melt. However, especially the z_{830} values can be relatively high in high accumulation regions along the coast, particularly in West Antarctica and the Antarctic Peninsula. In these regions, the accumulation is so high that the fast burial of snow leads to a thick firn layer despite the mild temperatures. The z_{550} and z_{830} values are also low in relatively warm and dry regions on and around Ross, Filchner Ronne and Amery ice shelf, where fresh snow is buried more slowly, and the densification rates are high due to relatively high temperatures. The measurements show that the model captures the spatial variations in z_{550} and z_{830} well.

Figure 4d shows the age of firn at the pore close off depth, here assumed to equal z_{830}. The combination of strongly increasing firn depth and decreasing accumulation towards the interior leads to firn ages at close-off depth that exceed 2000 years in central East Antarctica, whereas the pore close-off firn age in warm and wet coastal margins can be as low as 20 years. These data are

https://doi.org/10.5194/tc-2022-118
Preprint. Discussion started: 20 July 2022

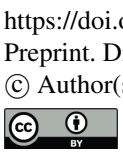

The Cryosphere Discussions
Open Access
EGU

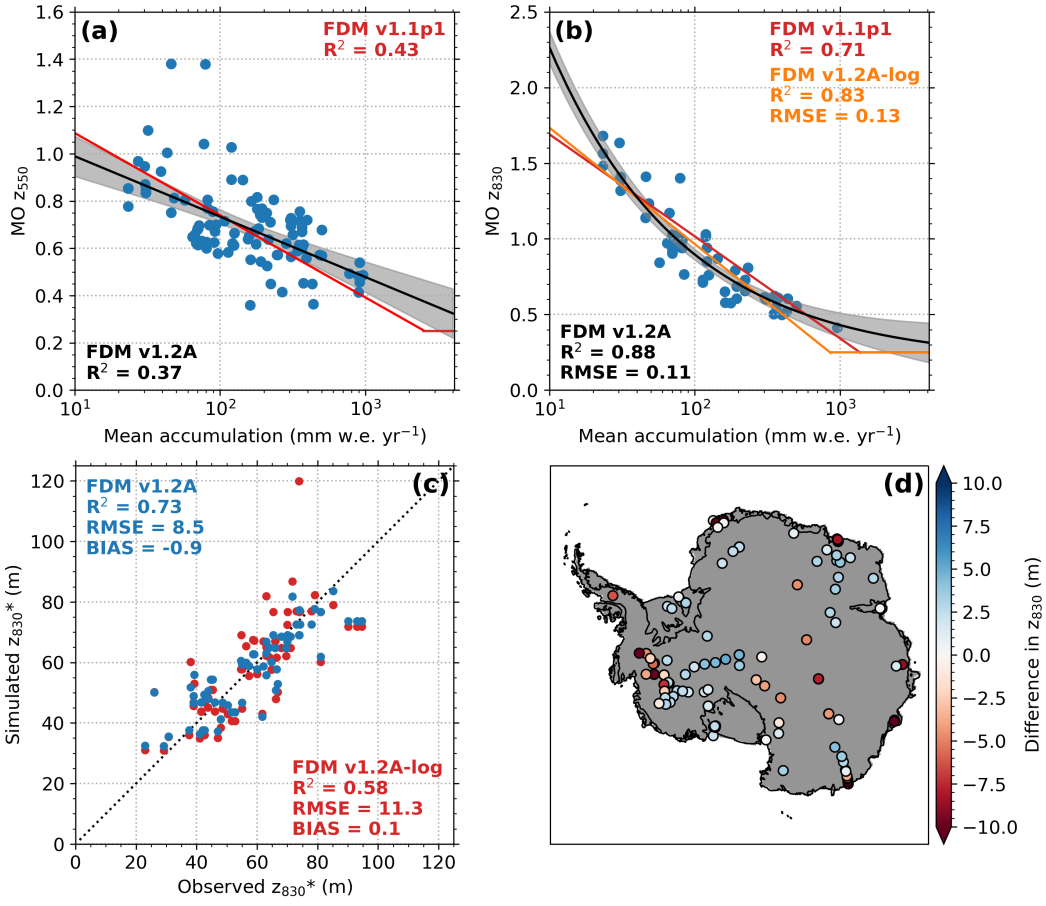

Figure 3. Scatter plots defining the MO ratios for **(a)** z_{550} and **(b)** z_{830} as a function of the annual average accumulation including various MO fits. The grey areas indicate the 95 % confidence intervals. **(c)** Scatter plots of the simulated against observed z_{830*} (z_{830}-z_{550}) for FDM v1.2A and FDM v1.2A-log. **(d)** Map of the difference in between simulated firn thickness (z_{830}) of the two tests (FDM v1.2A – FDM v1.2A-log) for locations with observations. The statistics and fits of the MO fits are listed in Table 3.

useful for the interpretation of the difference between the age of air in the bubbles and the ice that encloses the bubbles (delta age; Blunier and Schwander, 2000).

4.2 Firn air content

Firn air content (FAC), a measure of the total (vertically integrated) pore space, is an important output of firn models as it can be used to convert volume changes to mass changes in mass balance studies and is an indicator of the meltwater buffering capacity of the firn. The firn air content is expressed in m and represents the change in depth that would occur if the firn layer would be compressed to the density of glacier ice. The average firn air content of the AIS according to IMAU-FDM is 22.8 m, and it varies spatially between 0 to 40 m across climatic regions (Fig. 5a). The pattern resembles the z_{830} pattern (Fig. 4c); thick

https://doi.org/10.5194/tc-2022-118
Preprint. Discussion started: 20 July 2022

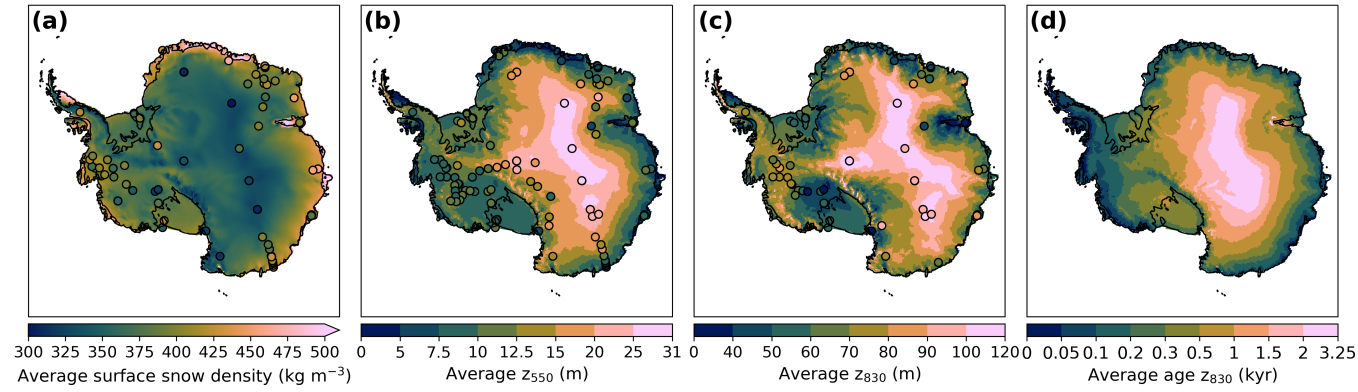

Figure 4. Maps from FDM v1.2A of the average **(a)** surface snow density (defined as the top 0.5 m), depths of critical density levels of **(b)** $\rho = 550$ kg m^{-3} (z_{550}) and of **(c)** $\rho = 830$ kg m^{-3} (z_{830}) (the firn thickness), and **(d)** firn age of the critical density level of (c) $\rho = 830$ kg m^{-3}. Circles indicate the values found by field measurements.

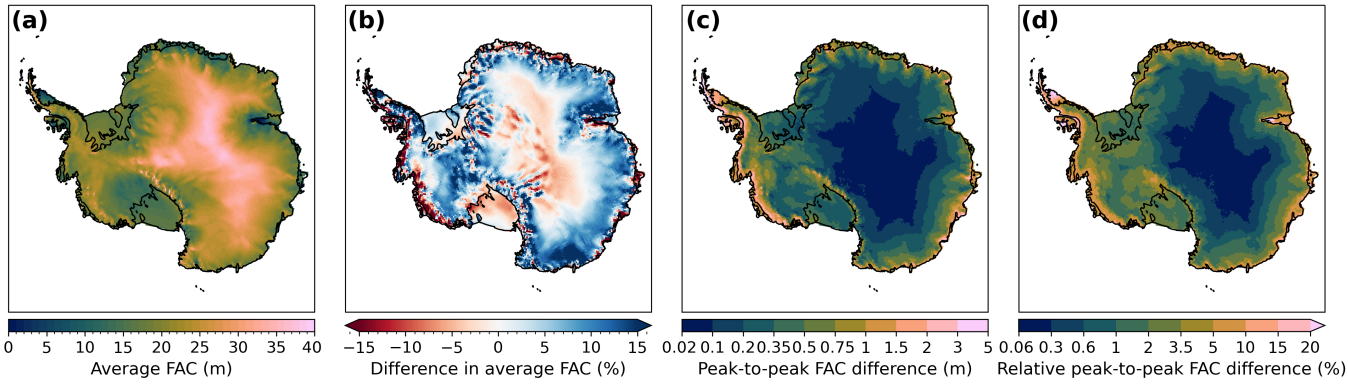

Figure 5. Maps from FDM v1.2A of average **(a)** firn air content (FAC), **(b)** the difference in FAC (FDM v1.2A - FDM v1.1p1), **(c)** peak-to-peak FAC difference, **(d)** relative peak-to-peak FAC difference compared to the average FAC from (a).

firn layers contain most air. High values are found in the cold interior and along parts the coast, particularly in West-Antarctica, and in parts with very high accumulation. Low values are found along the warmer coastal margins, with ice shelves having an average FAC of 15.9 m. These average FAC estimates are somewhat lower compared to values simulated with the CFM forced with MERRA-2 climate data of 24.9 and 19.4 m respectively (Medley et al., 2020), which might be explained by higher accumulation rates in their forcing data.

The average FAC over the entire AIS (including the ice shelves) simulated with FDM v1.2A is 0.6 m higher than simulated with FDM v1.1. The significant spatial FAC differences between FDM v1.2A and FDM v1.1 are shown Figure 5b. In the highly elevated and low accumulation regions the new FAC is lower, whereas in the intermediate accumulation regions the new FAC is higher. This implies that the range of FAC is smaller and closer to the mean than previously modelled. The differences in

https://doi.org/10.5194/tc-2022-118
Preprint. Discussion started: 20 July 2022

FAC pattern can be explained by differences in the (i) MO_{830} fit, (ii) fresh snow density, (iii) snowfall and (iv) snowmelt. FDM v1.2A has higher MO_{830} values for low and high accumulation regions compared to FDM v1.2A, which results in a faster densification and therefore lower FAC values. In intermediate accumulation regions the MO_{830} values are lower, resulting in a slower densification and higher FAC values. The fresh snow densities of FDM v1.2A are on average lower (Fig. 2), which contributes to FAC values being higher on average. On top of that, increased snowfall in the interior and increased snowmelt along the coastal margins in RACMO2.3p2 compared to RACMO2.3p1 (Van Wessem et al., 2018), also contributes to the general pattern of higher FAC in the interior and lower values along the coastal margins.

Figures 5c and d focus on temporal variability in FAC. Figure 5c shows the peak-to-peak FAC difference, that represents the difference between the highest and the lowest FAC value occurring during the study period. Large values indicate that seasonal and interannual climate variability cause large temporal variations in FAC. The peak-to-peak FAC difference is low in the interior, less than 0.1 m, despite the high FAC. Along the coastal margins, the peak-to-peak FAC difference is higher, up to 5 m, even though the FAC is generally lower. Therefore, the relative peak-to-peak FAC difference is low in the interior (<1 %) and high near the ice sheet margins (>5 %) (Fig. 5d). The average relative peak-to-peak FAC difference for the ice shelves, excluding the two largest ones, the Ross and Ronne-Filchner ice shelves, amounts to 13 %. The high peak-to-peak variability is caused by a combination of significant temporal variability in accumulation and melt. The temporal firn variability and the driving processes are discussed further in Sections 4.3 and 4.4 below.

4.3 Seasonal firn air content and firn height variability

In order to better understand the FAC temporal variability and its drivers, we decompose the signal into seasonal and interannual contributions. Figure 6a shows the average seasonal cycle of the vertical firn surface velocity (V_{tot}) including its components from Eq. (6). Four main processes drive the seasonality of the firn thickness: snowfall (V_{snow}), firn densification (V_{fc}), melt (V_{melt}) and sublimation (V_{sub}). Snowfall is highest in winter, while firn densification, melt and sublimation peak in summer. The net result is that the firn thickness and firn air content steadily increase over the winter, due to enhanced accumulation and reduced firn densification, melt and sublimation (Fig. 6b). This is followed by a sharp decrease over the summer due to reduced accumulation and increased firn densification and melt. The firn height change by ice flux divergence (V_{ice}) is constant by definition, while the continental average impact of snowdrift (V_{snd}) and buoyancy (V_{buoy}) is negligible. The vertical bars in Figure 6a indicate the interannual variability, which is driven solely by snowfall except for the two summer months.

The average seasonal amplitudes of the firn thickness and FAC, defined as half the peak-to-peak values of the average seasonal cycle, are 3.5 and 2.4 cm, which amounts to Antarctic wide integrated volumes of 463 and 304 km^3, respectively. This agrees with the modelled firn thickness amplitude of 3.5 cm by Medley et al. (2020). The average seasonal peak-to-peak values of firn thickness and FAC, defined as the average difference between the highest and the lowest value of each year, are considerably higher, 13.5 and 8.5 cm, amounting to volume changes of 1784 and 1123 km^3, respectively (Fig. 6c). The difference between the seasonal amplitudes and peak-to-peak values is due to interannual variations in the timing of the seasonal maximum and minimum. The difference between the firn thickness and FAC seasonal cycles suggests that 63 to 68 % of the seasonal surface elevations fluctuations are caused by a change in air content rather than actual mass change. It

https://doi.org/10.5194/tc-2022-118
Preprint. Discussion started: 20 July 2022

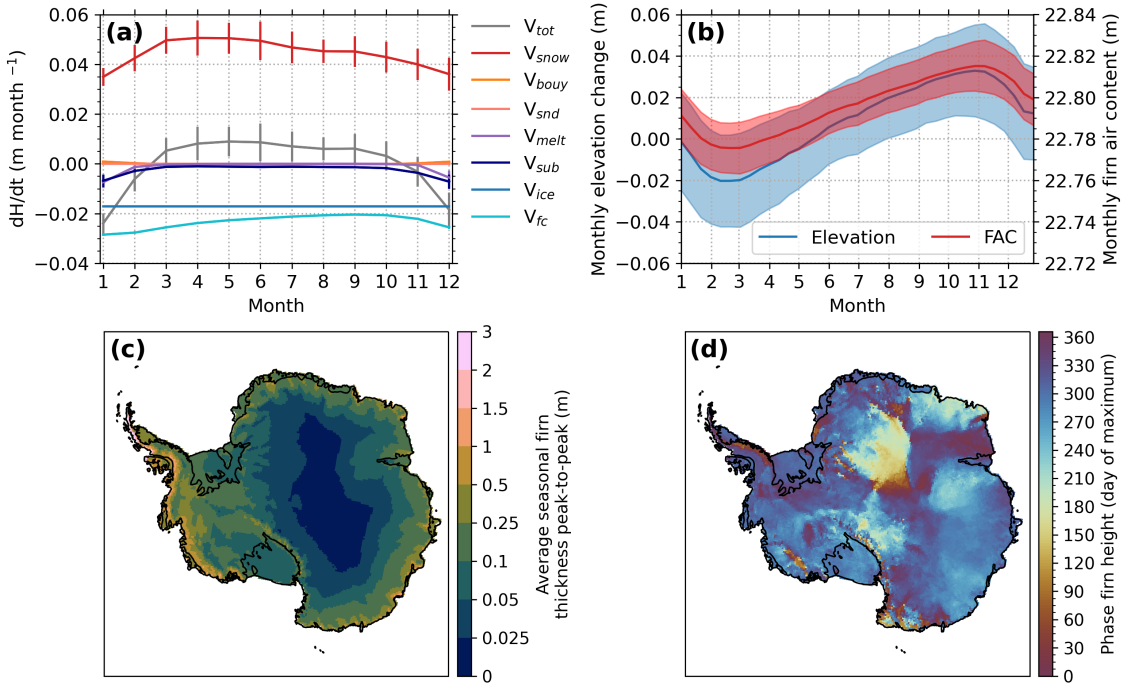

Figure 6. Ice sheet averaged seasonal cycle from FDM v1.2A of the **(a)** vertical firn surface velocity including its separate components from Eq. 6, and of **(b)** surface elevation change and firn air content (FAC). The bars and colored areas indicate the standard deviations. Maps from FDM v1.2A **(c)** of the average seasonal firn thickness peak-to-peak difference and **(d)** of timing of firn height phase maximum.

implies that not including the seasonal cycles of FAC in altimetry studies can generate significant biases, which emphasizes the importance of using firn densification models, especially when investigating shorter periods and regions with large seasonal SMB cycles.

Figure 6c shows that the seasonal peak-to-peak firn thickness change can be up to 3 m in the western Antarctic Peninsula, caused by a rare combination of substantial snowfall ánd melt. In regions with little melt, such as coastal West Antarctica, the values are typically 1 m. In the interior, values of less than 2.5 cm are found, as the annual average accumulation is low and melt absent. Figure 6d shows the average phase of the firn thickness maximum, which generally occurs during late winter or spring, before the summer decrease in accumulation and increase in temperature. In some regions accumulation peaks in late summer or early winter, e.g., along the Weddell Sea coast, in Enderby Land, Adélie Land and parts of the interior. Here, the the maximum firn depth occurs in late summer or early winter.

4.4 Interannual firn air content and firn height variability

Figure 7 shows time series of FAC and the cumulative surface temperature and vertical firn surface velocity anomalies including its components (Eq. 6). The figure confirms that the seasonal firn thickness and FAC variability is driven by snowfall,

https://doi.org/10.5194/tc-2022-118
Preprint. Discussion started: 20 July 2022

densification, melt and sublimation resulting in a firn thickness peak in late winter. The figure also reveals decadal firn thickness and FAC variability mainly resulting from fluctuations in snowfall, and that firn densification, despite the long time scale, reduces these snowfall-induced fluctuations by about 15 %. Generally, we observed that periods of significant snowfall and firn thickness fluctuations last 5 to 10 years. For example, from 2005 to 2015, decreased snowfall resulted in decreased firn thickness and FAC. We also find significant interannual variability in melt, but snowfall variability dominates. Below 2,000 m a.s.l. the variability in firn thickness and FAC are substantially larger, which can be attributed to the higher accumulation (70 % of the total accumulation falls on only 40 % of the ice sheet), in combination with variability of snowmelt and firn densification. Above 2,000 m a.s.l. the variability of firn densification is also relatively high, which can partly be explained by the larger temperature variability in this area. The interannual variability in snowfall and temperature are related to low- and mid-latitude climate oscillations such as the El Nino-Southern Oscillation and the Southern Hemisphere Annular Mode (Kwok and Comiso, 2002; Marshall et al., 2017). Figure 7 shows that the magnitude of the decadal FAC variability (sd = 1.8 cm) constitutes a large fraction (67 %) of the total surface elevation change (sd = 2.7 cm). This reiterates the necessity of the common practice to remove decadal variability in FAC from altimetry signals to avoid errors in mass change estimates.

5 Comparison with altimetry and FDM v1.1 surface elevation change

In sections 3.1, 3.2 and 4 we have shown that the model captures the strong spatial variation in firn thickness and density. To also evaluate the temporal variation, we compare our simulated elevation trends and seasonal variability to multi-mission satellite altimetry observations reported by Schröder et al. (2019) for the period 1992-2015. Our firn simulations only provide elevation change due to anomalies in firn thickness caused by variations in e.g. snow accumulation, surface temperature, firn densification and melt. The difference between the observed and simulated elevation change therefore represents a combination of elevation changes due to ice-dynamical imbalance, errors in the firn model and its climate forcing and errors in the altimetry observations. For this comparison, we therefore exclude regions with ice-dynamical imbalance, by using the ice-dynamical imbalance mask of Shepherd et al. (2019), which mainly consists of Pine Island, Thwaites, Totten and Getz glacier basins and the Kamb ice stream.

5.1 Seasonal amplitude

Ligtenberg et al. (2012) compared satellite altimetry and FDM v1.1p1 surface height seasonal variability. They found that FDM v1.1p1 patterns qualitatively agree with low variability in the interior and high variability near the margins (Fig. 6c), and that the significantly lower seasonal variability of FDM v1.1p1 compared to satellite altimetry can likely be explained by altimetry errors. The altimetry observations prior to 2003 exhibit a larger short-term variability as a result of the lower measurement precision of the satellites during that period, and are excluded from the analysis here. To enable comparison with the FDM v1.1p1 simulation, we focus on the period 2003-2015. To reduce the impact of the long-term trends we remove a linear trend from all datasets. After doing so, we find that the seasonal amplitude averaged over the ice sheet of the altimetry observations amounts to 5.2 cm, of the FDM v1.2A simulations to 3.1 cm (60 % of the observed amplitude) and of the FDM

https://doi.org/10.5194/tc-2022-118
Preprint. Discussion started: 20 July 2022

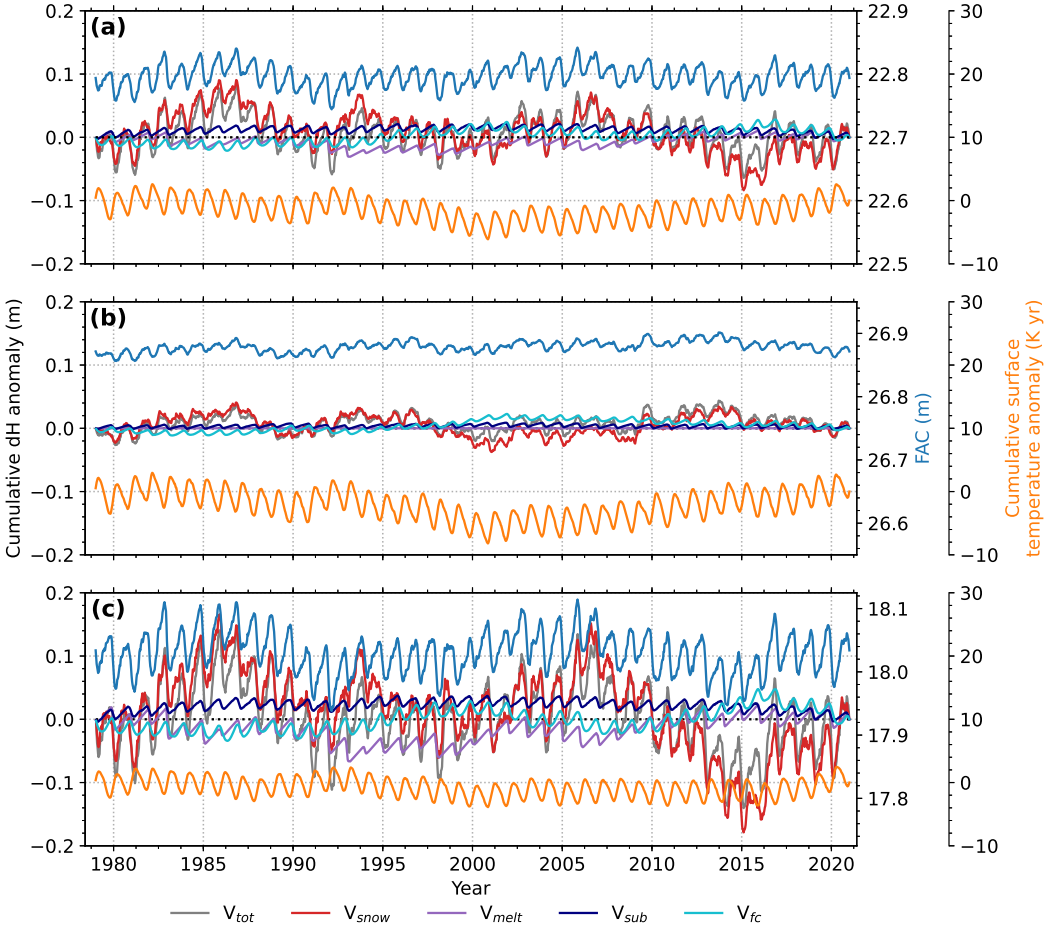

Figure 7. Time series from FDM v1.2A of FAC and the cumulative anomalies of surface temperature and the vertical firn surface velocity including its separate components from Eq. (6) for **(a)** the entire ice sheet, **(b)** the part of the ice sheet situated above 2,000 m a.s.l. and **(c)** the part of the ice sheet situated below 2,000 m a.s.l.

v1.1p1 simulations to 2.5 cm (48 % of the observed amplitude). The performance of the new model thus appears to represent an improvement, which results from increased snowmelt along the coastal margins of RACMO2.3p2 compared to RACMO2.3p1 in combination with a lower fresh snow density (Fig. 2).

5.2 Decadal variability

In Figure 8 we compare observed (Fig. 8a) and simulated 2003-2015 average surface elevation change. To obtain these numbers, a linear regression is used. The FDM v1.2A surface elevation change over this period is positive in Dronning Maud Land, Enderby Land, and negative in most other regions (Fig. 8b). FDM v1.1p1 (Fig. 8c) has roughly similar patterns as FDM v1.2A, but the regional amplitudes differ. Figure 8d shows the residual surface elevation change of FDM v1.2A, which is calculated

https://doi.org/10.5194/tc-2022-118
Preprint. Discussion started: 20 July 2022

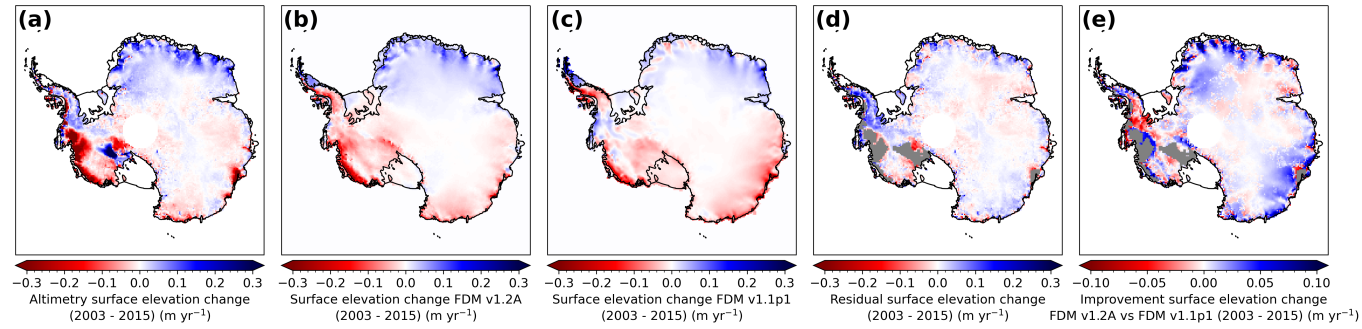

Figure 8. Maps of average surface elevation change over the period 2003-2015 from **(a)** multi-mission altimetry (Schröder et al., 2019), **(b)** FDM v1.2A and **(c)** FDM v1.1p1 obtained using linear regression. **(d)** Residual trend of FDM v1.2A minus altimetry. **(e)** Improvement of the FDM v1.2A trend compared to FDM v1.1p1. Regions within the ice-dynamical imbalance mask reported by Shepherd et al. (2019) are excluded in **(d)** and **(e)** and indicated by the grey shaded area.

as the difference between the altimetry and FDM v1.2A elevation change and thus combines the errors in the firn model and altimetry. In Figure 8e we subtracted the absolute residual surface elevation change of FDM v1.2A and of FDM v1.1p1 from each other, which yields the improvement of FDM v1.2A compared to FDM v1.1p1. In Figures 8d and e, regions with ice-dynamical imbalance are excluded. The surface elevation change of FDM v1.2A has improved in most regions, especially in Dronning Maud Land, Wilkins Land and Adélie Land, where the FDM v1.2A trend has become either more positive or less negative. The residual absolute trend of FDM v1.2A has been reduced by 17 % compared to FDM v1.1p1 (from 2.6 to 2.1 $\mathrm{cm\,yr^{-1}}$). In the Antarctic Peninsula and Ellsworth Land the agreement of FDM v1.2A with altimetry has reduced compared to FDM v1.1p1. In these regions, a substantial residual positive trends remains (>10 $\mathrm{cm\,yr^{-1}}$) (Fig. 8d), which might be due to an increase in accumulation on centennial time scales in these regions (e.g., Thomas et al., 2015, 2017). This implies that the actual firn column is not in balance with the 1979-2020 climate, and that the accumulation used for our spin-up period, which we assumed to be equal to 1979-2020 average accumulation, is overestimated in these regions. As a result, the vertical downward ice flow (Eq. 6) is overestimated, which results in underestimated surface elevation change.

In Figure 9 we compare time series of altimetry observed elevation change over the period 1992-2015 to simulated elevation change for eleven representative locations across the AIS. The time series have been smoothed using a 6-monthly moving average window. At most locations, FDM v1.2A shows comparable patterns to the observations, and the agreement seems to have been improved compared to FDM v1.1p1. This improvement is mainly due to changes in the RACMO2.3p2 forcing, given the strong similarity between elevation change of FDM v1.2A and FDM v1.1p2. As in Figure 8, we find a substantial residual altimetry trend (>10 $\mathrm{cm\,yr^{-1}}$) at location 5 (Antarctic Peninsula). At locations 1 (Dronning Maud Land) and 6 (Ellsworth Land) we find a minor residual altimetry trend ($\sim$5 $\mathrm{cm\,yr^{-1}}$). The altimetry observations prior to 2003 exhibit relatively stronger short-term variability (+9 % sd), likely related to the measurement imprecision. The agreement with FDM v1.2A also appears to increase after 2003, however the altimetry variability remains higher than the simulated variability (+13 % sd).

https://doi.org/10.5194/tc-2022-118
Preprint. Discussion started: 20 July 2022

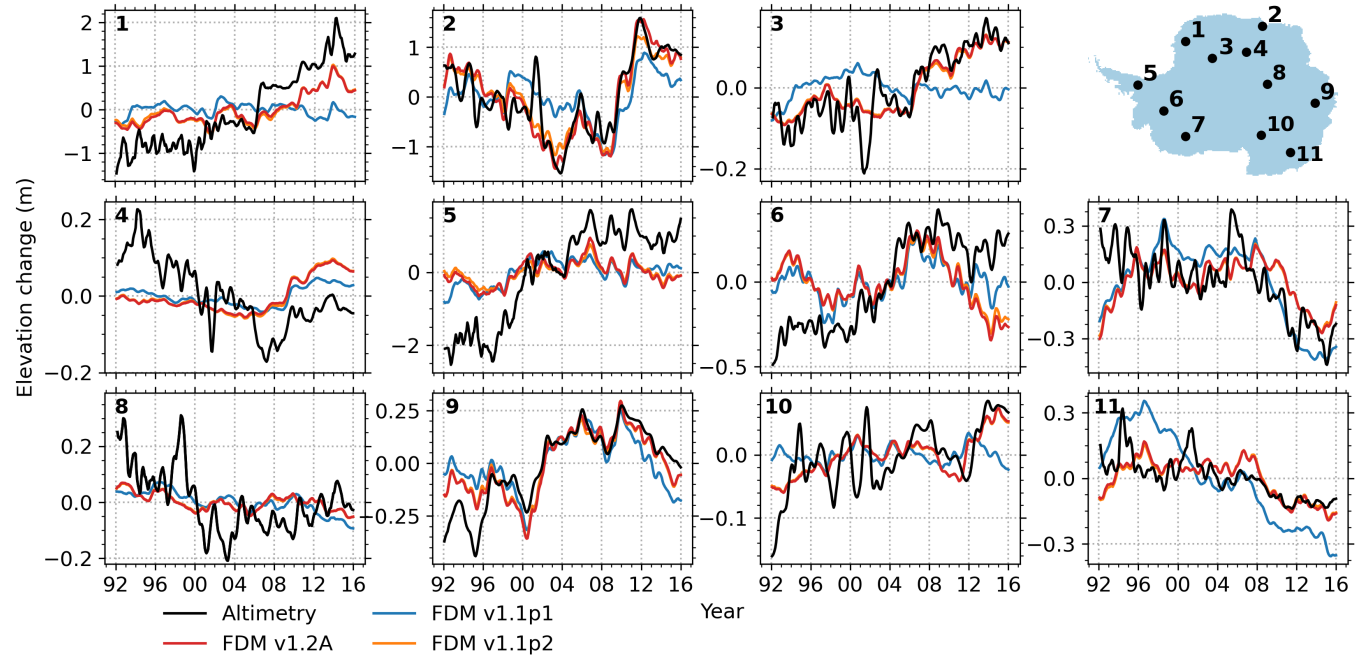

Figure 9. Time series of the altimetry observed and modelled elevation change for eleven locations over the period 1992-2015. The time series have been smoothed using a 6-monthly moving average window. The modelled elevation change includes FDM v1.2A, FDM v1.1p1 and FDM v1.1p2. The number of each panel corresponds to the numbered locations on the maps.

6 Uncertainty analysis

We investigated the impacts of uncertainties in the climate forcing, model densification expressions and fresh snow density on our final FAC, z_{550}, and z_{830} results (Table 4). Note that, if we initially would have had a different forcing and fresh snow density, we would also have obtained different MO fits (Eq. 4 and 5). Therefore, we performed additional model runs in which we also adjusted the MO fits. With the original MO fits, the FAC responds rather linearly to the imposed changes, with the highest sensitivity to the temperature uncertainties (+/-6 %) and the lowest sensitivity to the accumulation uncertainties (+/-2 %). The RMSE of the z_{550} and z_{830} somewhat increase. The FAC and RMSE of z_{550} and z_{830} sensitivity with the updated MO fits are substantially lower. These results suggest that our FAC, z_{550} and z_{830} estimates are robust.

As the model set up of our reference simulation assumes a steady-state firn layer, there is no net surface elevation trend in this simulation over the period 1979-2020. In the sensitivity tests in which the accumulation and temperature during the spin-up period are adjusted, the firn layer is not in steady state anymore, which results in surface elevation trends. The average surface elevation trend over the period 1979-2020 of the accumulation test amounts to +4 $\mathrm{cm\,yr^{-1}}$ (1.72 m in total) and of the temperature to -0.7 $\mathrm{cm\,yr^{-1}}$ (-0.3 m in total). As the temperature and accumulation have opposite effects, the test in which accumulation and temperature were adjusted simultaneously yields an average surface elevation trend of +3.3 $\mathrm{cm\,yr^{-1}}$ (1.36 m

https://doi.org/10.5194/tc-2022-118
Preprint. Discussion started: 20 July 2022

Table 4. Overview of the change in annual average firn air content and change in RMSE of z_{550} and z_{830} with the adjusted inputs and parameters from FDM v1.2A, including the FAC and RSME of z_{550} and z_{830} of the reference run. The inputs and parameters are adjusted by subtracting and adding the uncertainties, which are described in Section 2.6.

Run (-/+ uncertainty)	With original MO fits			With updated MO fits		
	FAC (m)	RMSE z_{550} (m)	RMSE z_{830} (m)	FAC (m)	RMSE z_{550} (m)	RMSE z_{830} (m)
Reference run	22	2.20	8.51			
Accumulation -	-2.6	0.07	0.40	-0.2	0.06	0.01
Accumulation +	+2.6	-0.02	0.03	0.6	0.03	0.04
Temperature -	+6	0.19	0.14	+0.4	0	-0.06
Temperature +	-6.3	0.28	0.28	-0.5	0.07	-0.01
Fresh snow density -	+6.1	0.99	0.04	0.1	0	-0.01
Fresh snow density +	-5.4	1.02	0.05	-0.2	0.05	-0.02
MO fits -	+5.5	0.18	0.08			
MO fits +	-5.1	0.14	0.73			

in total). From linear regression between the surface elevation trend of the combined accumulation and temperature test and the annual average accumulation, we obtain a relation of 0.05 m total surface elevation change per 100 $\mathrm{mm\,yr^{-1}}$ accumulation (R^2 = 0.94). This means that in locations with >1000 mm annual average accumulation the elevation increases by >5 m over the period 1979-2020. If we focus on the period that we used for the remote sensing comparison in Figure 9 (1992-2015) we find that the surface elevation trends increase by +3.9 $\mathrm{cm\,yr^{-1}}$ (+0.93 m in total) for the accumulation test, decrease by -0.8 $\mathrm{cm\,yr^{-1}}$ (-0.18 m in total) for the temperature test and increase by +3.2 $\mathrm{cm\,yr^{-1}}$ (0.77 m in total) for the combined accumulation and temperature test. We conclude that FDM is most sensitive to the uncertainty in the accumulation during the spin-up period. Long-term increases in accumulation are mainly found in the Antarctic Peninsula, Ellsworth Land and to some extent in Dronning Maud Land, and for some regions over some periods even reduced accumulation has been found (Thomas et al., 2015, 2017). The long-term increases in accumulation partly explains the discrepancy between FDM and altimetry observations for these regions as is discussed in Section 5.2.

7 Remaining limitations and outlook

The comparison with in situ and remote sensing measurements and the sensitivity analysis showed that FDM in general performs well and that our results are robust. A difficulty of the data to model comparison is that, especially in the interior, both the long-term trend and seasonal variability are small compared to the error range of the altimetry observations, which explains part of the remaining discrepancy that exist there, but also hampers the comparison (Verjans et al., 2021). More accurate in situ measurements of surface height evolution and firn densification are sparse. Future evaluation of firn models will therefore likely

https://doi.org/10.5194/tc-2022-118
Preprint. Discussion started: 20 July 2022

continue dependent on satellite altimetry comparison. The ICESat-2 ATL15 (Smith et al., 2021) is a precise Antarctic-wide 3-month height change laser product that is available from May 2018 onwards, thereby providing an opportunity to assess seasonal and decadal variations, especially in the coming years when more data will become available. Smith et al. (2022) already used ICESat-2 measurements to evaluate regional climate and firn densification models in Greenland.

An important limitation of IMAU-FDM, which is evident from both the remote sensing comparison and the sensitivity analysis, is the assumption of a steady-state firn layer, which may be a poor assumption in e.g., the Antarctic Peninsula and Ellsworth Land. The steady increase in accumulation over the last centuries in these regions results in a positive surface elevation trend in these regions which can not be captured by the model. Correcting for this accumulation trend by estimating it from ice core data, could be a next step to improve this aspect of firn models.

8 Conclusions

In this study, we present and evaluate a simulation of the contemporary characteristics of the Antarctic firn layer using the updated IMAU-FDM (Firn Densification Model), version v1.2A, for the period 1979-2020. In this new version, the fresh snow density and firn compaction parameterizations have been improved, and an updated atmospheric forcing has been used. The RMSE when compared to observations of the fresh snow density and firn thickness have been reduced by 26 and 23 %, respectively, compared to the previous parameterizations. In general, the modelled fresh snow densities have decreased, especially in high accumulation areas and to a lesser extent in windy escarpment regions. Firn thickness and FAC have decreased in low- and high accumulation areas, whereas it has increased in intermediate accumulation areas.

In accordance with observations, the firn thickness and density patterns vary spatially across climatic regions with temperature as a primary and accumulation as a secondary driver. Along the coastal margins, we found that the firn thickness and firn air content vary strongly in time, whereas in the interior the variations are small. The temporal variations can be split into a rather stable seasonal cycle driven by snowfall, compaction, summer melt and sublimation, and more irregular decadal variations mainly driven by slow snowfall anomalies. As variations in firn air content and firn thickness align, 63 to 68 % of the seasonal and decadal surface height variability is due to variations in firn air content rather than firn mass, which emphasizes the importance of correcting for seasonal and decadal firn air content variations in altimetry studies. Comparison of simulated surface elevation change with altimetry shows that in most regions the modelled and observed trends agree reasonably well. The performance of the updated model has improved, notably in Dronning Maud Land and Wilkins Land, which is predominantly due to updated climate forcing. However, a significant trend difference remains in the Antarctic Peninsula and Ellsworth Land, which is likely caused by increasing accumulation over the past centuries, that violates the model assumption of a steady state over the simulated period (1979-2020). The altimetry comparison also suggests that the amplitude of the modelled seasonal cycle has somewhat improved compared to the previous model version. The sensitivity analysis shows that our model in general is robust, and that it is most sensitive to uncertainties in the accumulation during the spin-up period. We conclude that the improved model captures the strong spatial and temporal variation in firn conditions in Antarctica that have been previously observed in firn cores and satellite altimetry.

https://doi.org/10.5194/tc-2022-118
Preprint. Discussion started: 20 July 2022

Code and data availability. All FDM v1.2A code and data can be obtained from the authors without conditions.

Author contributions. SV, WJvdB, MB, PKM and MRvdB defined the research goals and designed the study. SV improved the model, performed the simulations and analyzed the results. All authors contributed to discussions on the manuscript.

Competing interests. MrvdB is a member of the editorial board of journal The Cryosphere

Acknowledgements. This work was funded by the Netherlands Organization for Scientific Research (grant no. OCENW.GROOT.2019.091). We acknowledge ECMWF for computational time on their supercomputers.

https://doi.org/10.5194/tc-2022-118
Preprint. Discussion started: 20 July 2022

References

Anderson, E. A.: A point energy and mass balance model of a snow cover., Stanford University, 1976.

Arthern, R. J., Vaughan, D. G., Rankin, A. M., Mulvaney, R., and Thomas, E. R.: In situ measurements of Antarctic snow compaction compared with predictions of models, Journal of Geophysical Research: Earth Surface, 115, https://doi.org/10.1029/2009JF001306, 2010.

Blunier, T. and Schwander, J.: Gas enclosure in ice: age difference and fractionation, in: Physics of Ice Core Records, pp. 307–326, Hokkaido University Press, 2000.

Bréant, C., Martinerie, P., Orsi, A., Arnaud, L., and Landais, A.: Modelling firn thickness evolution during the last deglaciation: constraints on sensitivity to temperature and impurities, Climate of the Past, 13, 833–853, https://doi.org/10.5194/cp-13-833-2017, 2017.

Brils, M., Kuipers Munneke, P., van de Berg, W. J., and van den Broeke, M.: Improved representation of the contemporary Greenland ice sheet firn layer by IMAU-FDM v1. 2G, Geoscientific Model Development Discussions, pp. 1–28, https://doi.org/10.5194/gmd-2021-303, 2021.

Brun, E., Martin, E., and Spiridonov, V.: Coupling a multi-layered snow model with a GCM, Annals of Glaciology, 25, 66–72, https://doi.org/10.3189/S0260305500013811, 1997.

Calonne, N., Milliancourt, L., Burr, A., Philip, A., Martin, C. L., Flin, F., and Geindreau, C.: Thermal Conductivity of Snow, Firn, and Porous Ice From 3-D Image-Based Computations, Geophysical Research Letters, 46, 13 079–13 089, https://doi.org/10.1029/2019GL085228, 2019.

Coléou, C., Xu, K., Lesaffre, B., and Brzoska, J.-B.: Capillary rise in snow, Hydrological processes, 13, 1721–1732, 1999.

Datta, R. T., Tedesco, M., Fettweis, X., Agosta, C., Lhermitte, S., Lenaerts, J. T., and Wever, N.: The effect of Foehn-induced surface melt on firn evolution over the northeast Antarctic peninsula, Geophysical Research Letters, 46, 3822–3831, https://doi.org/10.1029/2018GL080845, 2019.

Davis, C. H. and Poznyak, V. I.: The depth of penetration in Antarctic firn at 10 GHz, IEEE Transactions on Geoscience and Remote Sensing, 31, 1107–1111, https://doi.org/10.1109/36.263784, 1993.

Fausto, R. S., Box, J. E., Vandecrux, B., Van As, D., Steffen, K., MacFerrin, M. J., Machguth, H., Colgan, W., Koenig, L. S., McGrath, D., et al.: A snow density dataset for improving surface boundary conditions in Greenland ice sheet firn modeling, Frontiers in Earth Science, 6, 51, https://doi.org/10.3389/feart.2018.00051, 2018.

Favier, V., Krinner, G., Amory, C., Gallée, H., Beaumet, J., and Agosta, C.: Antarctica-regional climate and surface mass budget, Current Climate Change Reports, 3, 303–315, https://doi.org/10.1007/s40641-017-0072-z, 2017.

Fernandoy, F., Meyer, H., Oerter, H., Wilhelms, F., Graf, W., and Schwander, J.: Temporal and spatial variation of stable-isotope ratios and accumulation rates in the hinterland of Neumayer station, East Antarctica, Journal of glaciology, 56, 673–687, https://doi.org/10.3189/002214310793146296, 2010.

Fourteau, K., Martinerie, P., Faïn, X., Schaller, C. F., Tuckwell, R. J., Löwe, H., Arnaud, L., Magand, O., Thomas, E. R., Freitag, J., et al.: Multi-tracer study of gas trapping in an East Antarctic ice core, The Cryosphere, 13, 3383–3403, https://doi.org/10.5194/tc-13-3383-2019, 2019.

Gilbert, E. and Kittel, C.: Surface melt and runoff on Antarctic ice shelves at 1.5 C, 2 C, and 4 C of future warming, Geophysical Research Letters, 48, e2020GL091 733, https://doi.org/10.1029/2020GL091733, 2021.

Gossart, A., Helsen, S., Lenaerts, J., Broucke, S. V., Van Lipzig, N., and Souverijns, N.: An evaluation of surface climatology in state-of-the-art reanalyses over the Antarctic Ice Sheet, Journal of Climate, 32, 6899–6915, 2019.

Groot Zwaaftink, C., Cagnati, A., Crepaz, A., Fierz, C., Macelloni, G., Valt, M., and Lehning, M.: Event-driven deposition of snow on the Antarctic Plateau: analyzing field measurements with SNOWPACK, The Cryosphere, 7, 333–347, 2013.

Helsen, M. M., Van Den Broeke, M. R., Van De Wal, R. S., Van De Berg, W. J., Van Meijgaard, E., Davis, C. H., Li, Y., and Goodwin, I.: Elevation changes in Antarctica mainly determined by accumulation variability, science, 320, 1626–1629, 2008.

Hersbach, H., Bell, B., Berrisford, P., Hirahara, S., Horányi, A., Muñoz-Sabater, J., Nicolas, J., Peubey, C., Radu, R., Schepers, D., et al.: The ERA5 global reanalysis, Quarterly Journal of the Royal Meteorological Society, 146, 1999–2049, https://doi.org/10.1002/qj.3803, 2020.

Kaspers, K., Van de Wal, R., Van den Broeke, M., Schwander, J., Van Lipzig, N., and Brenninkmeijer, C.: Model calculations of the age of firn air across the Antarctic continent, Atmospheric Chemistry and Physics, 4, 1365–1380, https://doi.org/10.5194/acp-4-1365-2004, 2004.

Keenan, E., Wever, N., Dattler, M., Lenaerts, J., Medley, B., Kuipers Munneke, P., and Reijmer, C.: Physics-based SNOWPACK model improves representation of near-surface Antarctic snow and firn density, The Cryosphere, 15, 1065–1085, https://doi.org/10.5194/tc-15-1065-2021, 2021.

Kuipers Munneke, P., Ligtenberg, S., Noël, B., Howat, I., Box, J., Mosley-Thompson, E., McConnell, J., Steffen, K., Harper, J., Das, S., et al.: Elevation change of the Greenland Ice Sheet due to surface mass balance and firn processes, 1960–2014, The Cryosphere, 9, 2009–2025, https://doi.org/10.5194/tc-9-2009-2015, 2015.

Kwok, R. and Comiso, J. C.: Spatial patterns of variability in Antarctic surface temperature: Connections to the Southern Hemisphere Annular Mode and the Southern Oscillation, Geophysical Research Letters, 29, 50–1, https://doi.org/10.1029/2002GL015415, 2002.

Lehning, M., Bartelt, P., Brown, B., and Fierz, C.: A physical SNOWPACK model for the Swiss avalanche warning: Part III: Meteorological forcing, thin layer formation and evaluation, Cold Regions Science and Technology, 35, 169–184, https://doi.org/10.1016/S0165-232X(02)00072-1, 2002.

Lenaerts, J. T., Van den Broeke, M., Déry, S., Van Meijgaard, E., Van de Berg, W., Palm, S. P., and Sanz Rodrigo, J.: Modeling drifting snow in Antarctica with a regional climate model: 1. Methods and model evaluation, Journal of Geophysical Research: Atmospheres, 117, https://doi.org/10.1029/2011JD016145, 2012.

Ligtenberg, S., Helsen, M., and Van den Broeke, M.: An improved semi-empirical model for the densification of Antarctic firn, The Cryosphere, 5, 809–819, 2011.

Ligtenberg, S., Horwath, M., Van den Broeke, M., and Legrésy, B.: Quantifying the seasonal "breathing" of the Antarctic ice sheet, Geophysical Research Letters, 39, https://doi.org/10.1029/2012GL053628, 2012.

Ligtenberg, S., Kuipers Munneke, P., and Van den Broeke, M.: Present and future variations in Antarctic firn air content, The Cryosphere, 8, 1711–1723, https://doi.org/10.5194/tc-8-1711-2014, 2014.

Lundin, J. M., Stevens, C. M., Arthern, R., Buizert, C., Orsi, A., Ligtenberg, S. R., Simonsen, S. B., Cummings, E., Essery, R., Leahy, W., et al.: Firn model intercomparison experiment (FirnMICE), Journal of Glaciology, 63, 401–422, 2017.

Marshall, G. J., Thompson, D. W., and van den Broeke, M. R.: The signature of Southern Hemisphere atmospheric circulation patterns in Antarctic precipitation, Geophysical Research Letters, 44, 11–580, https://doi.org/10.1002/2017GL075998, 2017.

Medley, B., Neumann, T. A., Zwally, H. J., and Smith, B. E.: Forty-year simulations of firn processes over the Greenland and Antarctic ice sheets, The Cryosphere Discussions, pp. 1–35, https://doi.org/10.5194/tc-2020-266, 2020.

Montgomery, L., Koenig, L., and Alexander, P.: The SUMup dataset: compiled measurements of surface mass balance components over ice sheets and sea ice with analysis over Greenland, Earth System Science Data, 10, 1959–1985, https://doi.org/10.5194/essd-10-1959-2018, 2018.

https://doi.org/10.5194/tc-2022-118
Preprint. Discussion started: 20 July 2022

Mottram, R., Hansen, N., Kittel, C., van Wessem, J. M., Agosta, C., Amory, C., Boberg, F., van de Berg, W. J., Fettweis, X., Gossart, A., et al.: What is the surface mass balance of Antarctica? An intercomparison of regional climate model estimates, The Cryosphere, 15, 3751–3784, https://doi.org/10.5194/tc-15-3751-2021, 2021.

Munneke, P. K., Ligtenberg, S. R., Van Den Broeke, M. R., and Vaughan, D. G.: Firn air depletion as a precursor of Antarctic ice-shelf collapse, Journal of Glaciology, 60, 205–214, https://doi.org/10.3189/2014JoG13J183, 2014.

Noël, B., van de Berg, W. J., Van Wessem, J. M., Van Meijgaard, E., Van As, D., Lenaerts, J., Lhermitte, S., Kuipers Munneke, P., Smeets, C., Van Ulft, L. H., et al.: Modelling the climate and surface mass balance of polar ice sheets using RACMO2–Part 1: Greenland (1958–2016), The Cryosphere, 12, 811–831, https://doi.org/10.5194/tc-12-811-2018, 2018.

Olmi, R., Bittelli, M., Picard, G., Arnaud, L., Mialon, A., and Priori, S.: Investigating the influence of the grain size and distribution on the macroscopic dielectric properties of Antarctic firn, Cold Regions Science and Technology, 185, 103 254, https://doi.org/10.1016/j.coldregions.2021.103254, 2021.

Oppenheimer, M., Glavovic, B., Hinkel, J., van de Wal, R., Magnan, A. K., Abd-Elgawad, A., Cai, R., Cifuentes-Jara, M., Deconto, R. M., Ghosh, T., et al.: Sea level rise and implications for low lying islands, coasts and communities, 2019.

Rignot, E., Mouginot, J., Scheuchl, B., Van Den Broeke, M., Van Wessem, M. J., and Morlighem, M.: Four decades of Antarctic Ice Sheet mass balance from 1979–2017, Proceedings of the National Academy of Sciences, 116, 1095–1103, https://doi.org/10.1073/pnas.1812883116, 2019.

Sato, T., Kosugi, K., Mochizuki, S., and Nemoto, M.: Wind speed dependences of fracture and accumulation of snowflakes on snow surface, Cold Regions Science and Technology, 51, 229–239, https://doi.org/10.1016/j.coldregions.2007.05.004, 2008.

Schröder, L., Horwath, M., Dietrich, R., Helm, V., Van Den Broeke, M. R., and Ligtenberg, S. R.: Four decades of Antarctic surface elevation changes from multi-mission satellite altimetry, The Cryosphere, 13, 427–449, https://doi.org/10.5194/tc-13-427-2019, 2019.

Schwanck, F., Simões, J. C., Handley, M., Mayewski, P. A., Bernardo, R. T., and Aquino, F. E.: Drilling, processing and first results for Mount Johns ice core in West Antarctica Ice Sheet, Brazilian Journal of Geology, 46, 29–40, https://doi.org/10.1590/2317-4889201620150035, 2016.

Shepherd, A., Ivins, E., Rignot, E., Smith, B., Van Den Broeke, M., Velicogna, I., Whitehouse, P., Briggs, K., Joughin, I., Krinner, G., et al.: Mass balance of the Antarctic Ice Sheet from 1992 to 2017, Nature, 558, 219–222, https://doi.org/10.1038/s41586-018-0179-y, 2018.

Shepherd, A., Gilbert, L., Muir, A. S., Konrad, H., McMillan, M., Slater, T., Briggs, K. H., Sundal, A. V., Hogg, A. E., and Engdahl, M. E.: Trends in Antarctic Ice Sheet elevation and mass, Geophysical Research Letters, 46, 8174–8183, https://doi.org/10.1029/2019GL082182, 2019.

Smith, B., Fricker, H. A., Gardner, A. S., Medley, B., Nilsson, J., Paolo, F. S., Holschuh, N., Adusumilli, S., Brunt, K., Csatho, B., et al.: Pervasive ice sheet mass loss reflects competing ocean and atmosphere processes, Science, 368, 1239–1242, https://doi.org/10.5194/tc-5-809-2011, 2020.

Smith, B. E., Medley, B., Fettweis, X., Sutterley, T., Alexander, P., Porter, D., and Tedesco, M.: Evaluating Greenland Surface-Mass-Balance and Firn-Densification Data Using ICESat-2 Altimetry, The Cryosphere Discussions, pp. 1–24, https://doi.org/10.5194/tc-2022-44, 2022.

Smith, B., B. P. J. S. D. T. S. T. A. N., Harbeck, K., et al.: ATLAS/ICESat-2 L3B Gridded Antarctic and Arctic Land Ice Height Change, Version 1, 2021.

Sommer, C. G., Wever, N., Fierz, C., and Lehning, M.: Investigation of a wind-packing event in Queen Maud Land, Antarctica, The Cryosphere, 12, 2923–2939, https://doi.org/10.5194/tc-12-2923-2018, 2018.

https://doi.org/10.5194/tc-2022-118
Preprint. Discussion started: 20 July 2022

Steger, C. R., Reijmer, C. H., Van Den Broeke, M. R., Wever, N., Forster, R. R., Koenig, L. S., Kuipers Munneke, P., Lehning, M., Lhermitte, S., Ligtenberg, S. R., et al.: Firn meltwater retention on the Greenland ice sheet: A model comparison, Frontiers in Earth Science, 5, 3, https://doi.org/10.3389/feart.2017.00003, 2017.

Stenni, B., Curran, M. A., Abram, N. J., Orsi, A., Goursaud, S., Masson-Delmotte, V., Neukom, R., Goosse, H., Divine, D., Van Ommen, T., et al.: Antarctic climate variability on regional and continental scales over the last 2000 years, Climate of the Past, 13, 1609–1634, https://doi.org/10.5194/cp-13-1609-2017, 2017.

Sugiyama, S., Enomoto, H., Fujita, S., Fukui, K., Nakazawa, F., Holmlund, P., and Surdyk, S.: Snow density along the route traversed by the Japanese-Swedish Antarctic Expedition 2007/08, Journal of Glaciology, 58, 529–539, https://doi.org/10.3189/2012JoG11J201, 2012.

Thomas, E. R., Hosking, J. S., Tuckwell, R. R., Warren, R., and Ludlow, E.: Twentieth century increase in snowfall in coastal West Antarctica, Geophysical Research Letters, 42, 9387–9393, https://doi.org/10.1002/2015GL065750, 2015.

Thomas, E. R., Van Wessem, J. M., Roberts, J., Isaksson, E., Schlosser, E., Fudge, T. J., Vallelonga, P., Medley, B., Lenaerts, J., Bertler, N., et al.: Regional Antarctic snow accumulation over the past 1000 years, Climate of the Past, 13, 1491–1513, https://doi.org/10.5194/cp-13-1491-2017, 2017.

van den Broeke, M.: Depth and density of the Antarctic firn layer, Arctic, Antarctic, and Alpine Research, 40, 432–438, https://doi.org/10.1657/1523-0430(07-021)[BROEKE]2.0.CO;2, 2008.

van Kampenhout, L., Lenaerts, J. T., Lipscomb, W. H., Sacks, W. J., Lawrence, D. M., Slater, A. G., and van den Broeke, M. R.: Improving the representation of polar snow and firn in the Community Earth System Model, Journal of Advances in Modeling Earth Systems, 9, 2583–2600, 2017.

Van Wessem, J. M., Van De Berg, W. J., Noël, B. P., Van Meijgaard, E., Amory, C., Birnbaum, G., Jakobs, C. L., Krüger, K., Lenaerts, J., Lhermitte, S., et al.: Modelling the climate and surface mass balance of polar ice sheets using RACMO2–Part 2: Antarctica (1979–2016), The Cryosphere, 12, 1479–1498, https://doi.org/10.5194/tc-12-1479-2018, 2018.

Vandecrux, B., Mottram, R., Langen, P. L., Fausto, R. S., Olesen, M., Stevens, C. M., Verjans, V., Leeson, A., Ligtenberg, S., Kuipers Munneke, P., et al.: The firn meltwater Retention Model Intercomparison Project (RetMIP): evaluation of nine firn models at four weather station sites on the Greenland ice sheet, The Cryosphere, 14, 3785–3810, https://doi.org/10.5194/tc-14-3785-2020, 2020.

Verjans, V., Leeson, A., McMillan, M., Stevens, C., van Wessem, J. M., van de Berg, W. J., van den Broeke, M., Kittel, C., Amory, C., Fettweis, X., et al.: Uncertainty in East Antarctic firn thickness constrained using a model ensemble approach, Geophysical Research Letters, 48, e2020GL092 060, https://doi.org/10.1029/2020GL092060, 2021.

Willen, M., Broerse, T., Groh, A., Wouters, B., Kuipers Munneke, P., Horwath, M., van den Broeke, M., and Schröder, L.: Separating Long-Term and Short-Term Mass Changes of Antarctic Ice Drainage Basins: A Coupled State Space Analysis of Satellite Observations and Model Products, Journal of Geophysical Research: Earth Surface, 126, e2020JF005 966, https://doi.org/10.1029/2020JF005966, 2021.

Winstrup, M., Vallelonga, P., Kjær, H. A., Fudge, T. J., Lee, J. E., Riis, M. H., Edwards, R., Bertler, N. A., Blunier, T., Brook, E. J., et al.: A 2700-year annual timescale and accumulation history for an ice core from Roosevelt Island, West Antarctica, Climate of the Past, 15, 751–779, https://doi.org/10.5194/cp-15-751-2019, 2019.

Winther, J.-G., Jespersen, M. N., and Liston, G. E.: Blue-ice areas in Antarctica derived from NOAA AVHRR satellite data, Journal of Glaciology, 47, 325–334, https://doi.org/10.3189/172756501781832386, 2001.